© 2016. Published by The Company of Biologists Ltd | Journal of Cell Science (2016) 129, 2937-2949 doi:10.1242/jcs.186213

RESEARCH ARTICLE

Staphylococcus aureus recruits Cdc42GAP through recycling endosomes and the exocyst to invade human endothelial cells

Liane Rauch[1,*], Kirsten Hennings[1,*], Claudia Trasak[1], Anja Röder[1], Barbara Schröder[2,3], Friedrich Koch-Nolte[4], Felix Rivera-Molina[5], Derek Toomre[5] and Martin Aepfelbacher[1,‡]

ABSTRACT

Activation and invasion of the vascular endothelium by *Staphylococcus aureus* is a major cause of sepsis and endocarditis. For endothelial cell invasion, *S. aureus* triggers actin polymerization through Cdc42, N-WASp (also known as WASL) and the Arp2/3 complex to assemble a phagocytic cup-like structure. Here, we show that after stimulating actin polymerization staphylococci recruit Cdc42GAP (also known as ARHGAP1) which deactivates Cdc42 and terminates actin polymerization in the phagocytic cups. Cdc42GAP is delivered to the invading bacteria on recycling endocytic vesicles in concert with the exocyst complex. When Cdc42GAP recruitment by staphylococci was prevented by blocking recycling endocytic vesicles or the exocyst complex, or when Cdc42 was constitutively activated, phagocytic cup closure was impaired and endothelial cell invasion was inhibited. Thus, to complete invasion of the endothelium, staphylococci reorient recycling endocytic vesicles to recruit Cdc42GAP, which terminates Cdc42-induced actin polymerization in phagocytic cups. Analogous mechanisms might govern other Cdc42-dependent cell functions.

KEY WORDS: Cdc42GAP, Phagocytosis, Staphylococci, Endothelium, Recycling endosomes

INTRODUCTION

During bacteremia, pathogens activate and invade the vascular endothelium, which thereby might become leaky and dysfunctional (Deanfield et al., 2007; Lemichez et al., 2010). In the worst case, this leads to severe sepsis associated with high lethality (Goldenberg et al., 2011; Lee and Slutsky, 2010). Furthermore, by crossing the endothelial barrier, intravascular bacteria can cause focal complications like arthritis and meningitis (Edwards and Massey, 2011; Kim, 2008). Of note, the endothelium not only propagates intravascular infection but also actively engages in combating it, that is, by producing inflammatory cytokines, regulating leukocyte trafficking and eliminating invaded bacteria (Rauch et al., 2014; Schroder et al., 2006; Vestweber, 2015).

[1]Institute of Medical Microbiology, Virology and Hygiene, University Medical Center Hamburg-Eppendorf, Martinistrasse 52, Hamburg 20246, Germany. [2]Institute of Biological and Medical Imaging (IBMI), Helmholtz Zentrum München, Ingolstädter Landstraße 1, Neuherberg 85764, Germany. [3]Institute for Biological Imaging, Technical University of Munich, Arcisstrasse 21, Munich 80333, Germany. [4]Institute of Immunology, University Medical Center Hamburg-Eppendorf, Martinistrasse 52, Hamburg 20246, Germany. [5]Department of Cell Biology, Yale University School of Medicine, 333 Cedar Street, New Haven, CT 06510, USA.
*These authors contributed equally to this work

‡Author for correspondence (m.aepfelbacher@uke.de)

M.A., 0000-0003-2473-2970

Received 18 January 2016; Accepted 13 June 2016

Staphylococcus aureus is a major agent of blood stream infection and sepsis worldwide (Lowy, 1998). Activation and invasion of the vascular endothelium is thought to underlie the main symptoms of *S. aureus* sepsis (Kerrigan and McDonnell, 2015). Furthermore, *S. aureus* has a propensity to invade the endothelial lining of heart valves leading to valve colonization and bacterial endocarditis (Chorianopoulos et al., 2009). Animal models have revealed that intravascular *S. aureus* preferentially attaches to the endothelium of postcapillary venules (Laschke et al., 2005).

In vitro and *in vivo S. aureus* invades endothelial cells through its surface-exposed fibronectin-binding proteins A and B (FnBPA and FnBPB) (Que et al., 2005; Schroder et al., 2006; Sinha et al., 2000). The FnBPs bind to host fibronectin and thereby activate α5β1 integrin signaling in the infected cells (Schroder et al., 2006; Sinha et al., 2000, 1999). FnBPA-induced integrin signaling triggers complex actin rearrangements in endothelial cells through the Rho-family GTP-binding protein Cdc42, its downstream effector N-WASp (also known as WASL) and the Arp2/3 complex (Schroder et al., 2006). Initially, actin comet tails are generated that propel the staphylococci on the endothelial cell surface and thereafter phagocytic-cup-like actin structures are assembled that pull the bacteria inside the cells (Freeman and Grinstein, 2014; Schroder et al., 2006).

Recently, a positive-feedback loop for Cdc42 activation was revealed in which actin filaments attached to fibronectin-activated β1-integrins recruit a guanine nucleotide exchange factor (GEF) for Cdc42. The GEF activates Cdc42 which induces further actin filament formation through N-WASp and the Arp2/3 complex leading to more GEF recruitment (Orchard et al., 2012). Such a positive-feedback loop might be responsible for the overshooting actin polymerization in the FnBPA-triggered comet tails. However, many actin-dependent cell functions can only be completed when the initial process of actin polymerization is eventually switched off. For instance, after contributing to the formation of the actin cup, Cdc42 activity has to be downregulated and filamentous actin in the phagocytic cup has to depolymerized before phagosome maturation can proceed in neutrophils (Beemiller et al., 2010; Lerm et al., 2007). Presently, it is largely unknown which molecular pathways and spatiotemporal dynamics govern downregulation of actin polymerization during bacterial invasion and/or phagocytosis.

Cdc42, like essentially all Rho-like GTP-binding proteins, is activated by GEFs that increase its GTP loading and inactivated by GTPase-activating proteins (GAPs) that enhance its intrinsic GTPase activity (Symons and Settleman, 2000). It is interesting to note, that certain cell functions require Cdc42 cycling between its GDP-bound and GTP-bound states (Etienne-Manneville, 2004; Symons and Settleman, 2000). Cdc42GAP (also termed p50RhoGAP, RhoGAP1 or ARHGAP1) belongs to the large group of GAPs for Rho family GTP-binding proteins and preferentially inactivates Cdc42 in cells (Barfod et al., 1993;

Journal of Cell Science (2016) 129, 2937-2949 doi:10.1242/jcs.186213

Lancaster et al., 1994). Cells from Cdc42GAP-knockout mice display hyperactivation of Cdc42, which is associated with impaired cell migration (Szczur et al., 2006; Wang et al., 2005, 2006; Yang et al., 2006). In Cdc42GAP-knockout neutrophils, the migratory defect has been attributed to deregulated cell polarization (Szczur et al., 2006). On the subcellular level Cdc42GAP has been found to associate with the leading edge of polarizing cells as well as with membrane compartments positive for the recycling endosome marker Rab11 (Shen et al., 2008; Sirokmany et al., 2006).

Rab11-positive recycling endosomes, in conjunction with the exocyst complex, have been implicated in polarity control of various cell types (Hertzog and Chavrier, 2011; Letinic et al., 2009). The exocyst complex consists of eight components (Sec3, Sec5, Sec6, Sec8, Sec10, Sec15, Exo70 and Exo84) and functions by tethering exocytic vesicles, including recycling endocytic vesicles, to specific sites at the plasma membrane (Hertzog and Chavrier, 2011; Munson and Novick, 2006). It has previously been demonstrated that tethering of vesicles by the exocyst precedes their fusion with the acceptor membrane (Rivera-Molina and Toomre, 2013). In animal cells, the exocyst complex is, among other proteins, regulated by Cdc42 and its homolog TC10 (also known as RhoQ) (Wu et al., 2008).

In this study, we investigated how staphylococci initiate a concerted action of Cdc42GAP, recycling endosomes and the exocyst complex to downregulate Cdc42-triggered actin polymerization in phagocytic cups and complete endothelial cell invasion.

RESULTS

S. aureus FnBPA-expressing particles recruit Cdc42GAP during invasion of human endothelial cells

The mechanisms by which bacteria stimulate actin polymerization to invade host cells have been extensively investigated (Carabeo, 2011). Although the transient and dynamic nature of filamentous (F)-actin reorganization during bacterial invasion also infers specific pathways that downregulate actin polymerization, very little is known about the underlying molecular mechanisms. We have previously demonstrated that, for endothelial cell invasion, the *S. aureus* integrin-activating adhesin FnBPA stimulates actin polymerization through the GTP-binding protein Cdc42, its downstream effector N-WASp and the Arp2/3 complex (Schroder et al., 2006). Here, we asked whether Cdc42GAP, a ubiquitous negative regulator of Cdc42, is also involved in endothelial cell invasion by *S. aureus*.

We first tested whether Cdc42GAP is recruited by *S. aureus* (strain Cowan I) upon infection of primary human umbilical vein endothelial cells (HUVECs). For this, endogenous Cdc42GAP and the extracellularly localized portion of the bacteria were stained for immunofluorescence in parallel. Cdc42GAP localized to both extracellular and intracellular bacterial tetrades that are typical for *S. aureus* (Fig. 1A). Likewise, GFP–Cdc42GAP, when expressed in the endothelial cells, translocated to clusters of *S. aureus* that were invading the cells (Fig. 1B). That endogenous Cdc42GAP and GFP–Cdc42GAP frequently localized to both the extracellular and intracellular staphylococci of the same bacterial cluster suggests that Cdc42GAP plays a role during the internalization process (Fig. 1A,B).

We next tested recruitment of GFP–Cdc42GAP-R305/6A, a GAP-activity deficient construct that does not elicit side effects upon overexpression, to *S. aureus* strains Cowan I, 8325-4 and DU5883 (Sinha et al., 2000). DU5883 is a derivative of strain 8325-4 that lacks FnBPA and FnBPB (Sinha et al., 2000). Strains Cowan I and 8325-4 but not DU5883 recruited GFP–Cdc42GAP-R305/6A suggesting that FnBPA and FnBPB are required for Cdc42GAP recruitment. Furthermore, DU5883 complemented with FnBPA or FnBPB, *Staphylococcus carnosus* heterologously expressing FnBPA (*FnBPA-S. carnosus*) and latex beads (1- and 3-µm diameter) coated with recombinant GST–FnBPA (FnBPA beads), but wild-type *S. carnosus* or GST-coated beads did not recruit GFP–Cdc42GAP-R305/6A (Fig. 1C; Sinha et al., 2000). Unspecific recruitment of overexpressed mCherry to phagocytic cups (i.e. by a so-called 'volume effect') was minor compared to the recruitment of GFP–Cdc42GAP-R305/6A (Fig. S1A). Taken together, these results indicate that FnBPs are necessary and sufficient to trigger Cdc42GAP recruitment in *S.-aureus*-infected HUVECs. To ensure that the FnBPA–fibronectin–integrin signaling axis is exclusively stimulated in HUVECs, *FnBPA-S. carnosus* and FnBPA beads were preferentially employed in this study (Sinha et al., 2000). FnBPA beads of 1-µm and 3-µm diameter were found to be best suited for quantifying internalization and visualizing protein recruitment, respectively.

In order to identify the region(s) of Cdc42GAP required for recruitment by invading *FnBPA-S. carnosus*, we expressed GFP–Cdc42GAP constructs lacking specific functional domains or activities in HUVECs (Fig. 1D). Loss of (1) the GAP activity (GFP–Cdc42GAP-R305/6A), (2) the GAP domain (GFP–Cdc42GAPΔGAP), (3) the polyproline region (GFP–Cdc42GAPΔPPro) or (4) the polyproline region and GAP domain (GFP–Cdc42GAPΔPProΔGAP), which leaves the Sec14 homology domain intact, did not significantly affect recruitment by the bacteria (Fig. 1C,D). In contrast, a construct lacking the Sec14 homology domain (GFP–Cdc42GAPΔSec14) showed essentially no recruitment (Fig. 1D). Specific enrichment of the GFP–Cdc42GAP constructs was verified by intensity plots across the bacterial clusters (Fig. 1D). Thus, the Sec14 homology domain, which is known to bind to phosphatidylinositol phosphates (Krugmann et al., 2002), is both necessary and sufficient for Cdc42GAP recruitment. We conclude that during endothelial cell invasion FnBPA-expressing staphylococci recruit Cdc42GAP through its Sec14 homology domain.

Cdc42GAP regulates FnBPA-mediated endothelial cell invasion and phagocytic cup closure

To test whether Cdc42GAP plays a functional role in FnBPA-dependent invasion of HUVECs, we knocked it down by 77% and 89% using two different small interfering RNAs (siRNAs). Cdc42GAP knockdown inhibited FnBPA bead invasion of HUVECs by 33–50% (Fig. 2A). Binding of beads to cells was not altered by Cdc42GAP knockdown (Fig. S1B). This documents that Cdc42GAP plays an important role in FnBPA-mediated invasion of HUVECs. The phagocytic cup has been defined as a particle-engulfing structure connected to the extracellular space that, upon closure, develops into a phagosome, defined as a completely intracellular compartment. Because our invasion assay is based on differential immunofluorescence staining of the extracellular and intracellular portions of bacteria or beads, it discriminates particles in different stages of invasion: (1) that are completely extracellular, (2) that are partially internalized and (3) that are completely intracellular (Fig. 2B). To further verify that our method correctly identifies partially internalized beads, we challenged cells expressing the plasma membrane marker GFP–GPI with FnBPA beads and stained only the extracellular portions of the beads. A three-dimensional projection shows an invading bead that is for the most part enwrapped by plasma membrane. At the top of the bead, a

Journal of Cell Science (2016) 129, 2937-2949 doi:10.1242/jcs.186213

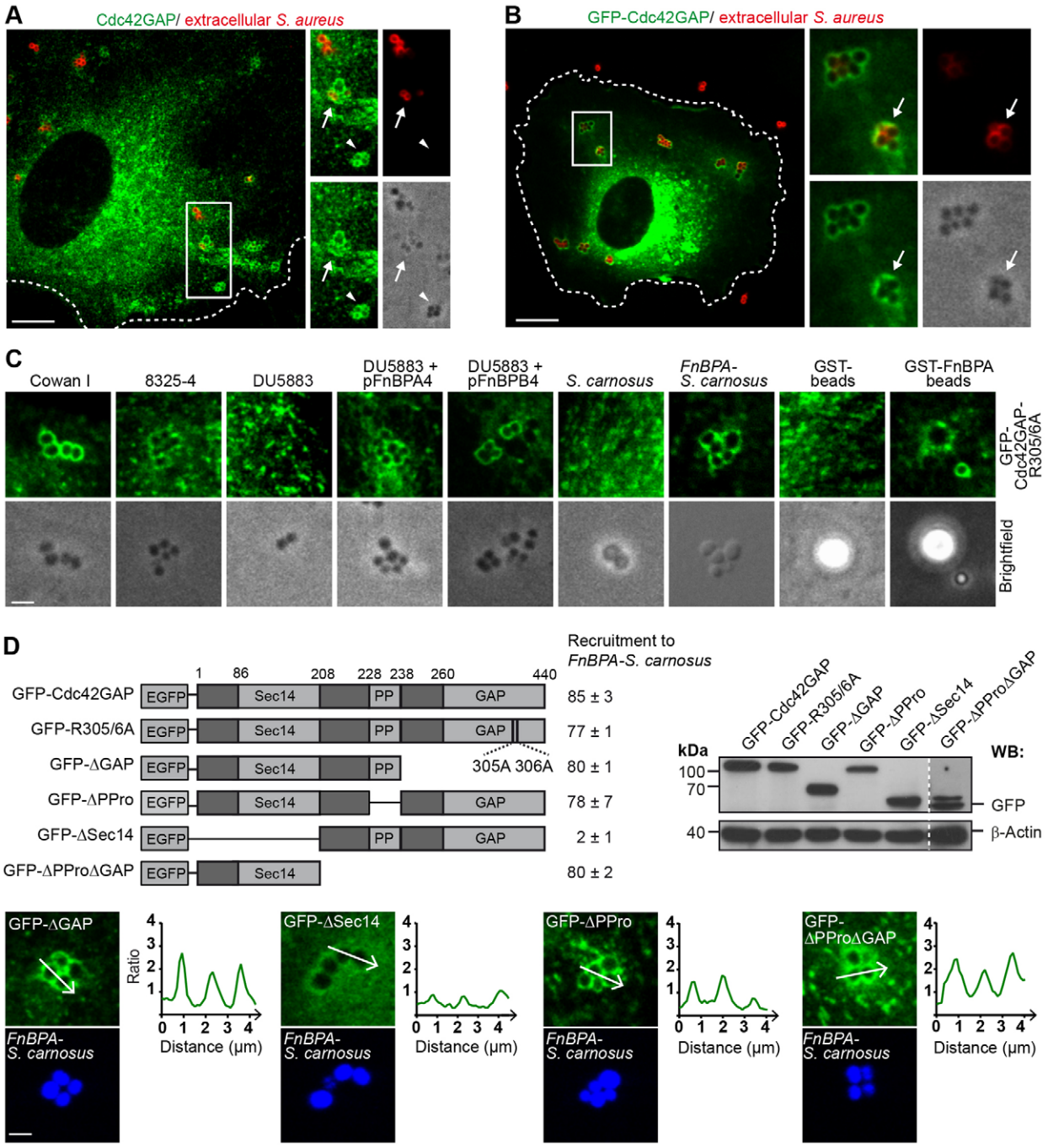

Fig. 1. Cdc42GAP is recruited to *S. aureus* during invasion of HUVECs. (A) HUVECs were infected with *S. aureus* (Cowan I) for 30 min and immunostained for endogenous Cdc42GAP (green) and extracellularly localized bacteria (red). The boxed region in the overview is depicted as a 1.5-fold enlargement in the right panels [overview (top left), extracellular bacteria (top right), endogenous Cdc42GAP (bottom left) and brightfield (bottom right)]. Cdc42GAP localization at an intracellular *S. aureus* cluster (white arrowhead) and a partially internalized cluster (white arrow) are highlighted. The cell border is indicated by the broken line. Scale bar: 10 µm. (B) HUVECs expressing GFP–Cdc42GAP were infected with *S. aureus* (Cowan I) for 30 min and extracellularly localized bacteria were immunostained (red). The boxed region in the overview is depicted as a 2.8-fold enlargement in the right panels [overview (top left), extracellular bacteria (top right), GFP–Cdc42GAP (bottom left) and brightfield (bottom, right)]. GFP–Cdc42GAP localization at a partially internalized cluster is indicated by the white arrow. The cell border is indicated by the broken line. Scale bar: 10 µm. (C) HUVECs expressing GFP–Cdc42GAP-R305/6A were challenged with *S. aureus* strain Cowan I, *S. aureus* strain 8325-4, *S. aureus* strain DU5883, *S. aureus* strain DU5883 complemented with plasmids pFnBPA4 or pFnBPB4, *S. carnosus* strain TM300, *S. carnosus* strain TM300 expressing FnBPA of 8325-4 (*FnBPA-S. carnosus*), or GST- and GST–FnBPA-coated beads (3-µm diameter) for 30 min. Scale bar: 2.5 µm. (D) Top left, scheme of GFP–Cdc42GAP constructs used in this study: GAP-activity-deficient arginine mutant (GFP-R305/6A); GAP-domain-deficient construct (GFP-ΔGAP); polyproline-region-deficient construct (GFP-ΔPPro); Sec14-domain-deficient construct (GFP-ΔSec14) and polyproline region plus GAP-domain-deficient construct (GFP-ΔPProΔGAP). Recruitment of GFP–Cdc42GAP constructs to *FnBPA-S. carnosus* is expressed as a percentage of cell-associated bacteria (mean±s.d.). At least 300 bacterial clusters from two different experiments were evaluated per construct. Recruitment was considered positive, when a clear intensity peak of fluorescence adjacent to the bacteria was detected versus background as shown in the intensity plots for GFP–ΔGAP, GFP–ΔPPro and GFP-ΔPProΔGAP in the lower panels. The intensity plot of GFP–ΔSec14 was considered as showing no specific recruitment. Scale bar: 2 µm. Top right, expression of GFP constructs was verified by anti-GFP western blotting (WB). A threefold higher exposure time was used for GFP–ΔPProΔGAP.

Journal of Cell Science (2016) 129, 2937-2949 doi:10.1242/jcs.186213

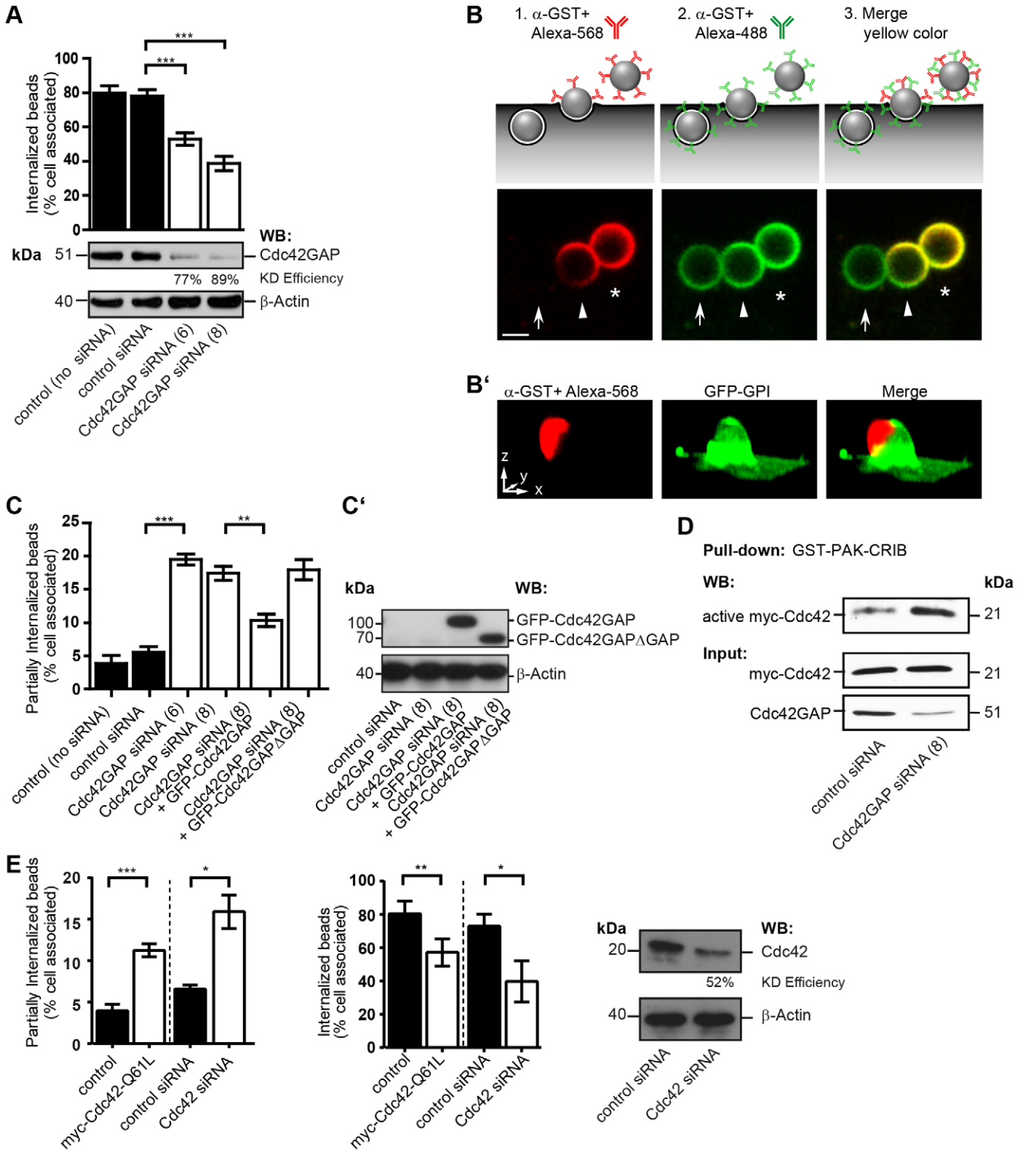

Fig. 2. See next page for legend.

cap not covered by membrane was stained by antibody (Fig. 2B′). This experiment strongly supports our assumption that plasma membrane that enwraps the bead during internalization prevents antibody access and produces the cap-like structures that identify partially internalized beads.

Interestingly, we observed that the fraction of beads that was partially internalized increased from ∼5% in controls to ∼20% in Cdc42GAP-knockdown cells (Fig. 2C). Overexpression of GFP–Cdc42GAP could largely rescue this effect of Cdc42GAP knockdown but overexpression of GFP–Cdc42GAPΔGAP could not (Fig. 2C,C′). Also, inhibition of FnBPA bead invasion by Cdc42GAP knockdown could be rescued by overexpression of Cdc42GAP but not of GFP–Cdc42GAPΔGAP (Fig. S1C). Therefore, the stage of the invasion process that is regulated by

Journal of Cell Science (2016) 129, 2937-2949 doi:10.1242/jcs.186213

Fig. 2. Knockdown of Cdc42GAP and Cdc42 hyperactivation inhibit phagocytic cup closure in FnBPA-mediated endothelial cell invasion. (A) HUVECs treated without (control) or with siRNAs specific for luciferase (control siRNA) or Cdc42GAP (siRNAs no. 6 and 8) for 72 h were challenged with FnBPA beads (1-µm diameter) for 30 min and immunostained for extracellular and intracellular beads. Bars represent mean±s.e.m.; 150–200 cells from at least three independent experiments were evaluated. ***P<0.0001 (one-way ANOVA with Bonferroni's post test). A representative western blot (WB) showing knockdown (KD) efficiency of Cdc42GAP siRNAs is also shown. (B) Schematic illustration of the double-staining method to distinguish between extracellular (asterisk), partially internalized (arrowhead) and intracellular (arrow) particles as shown in the lower images. FnBPA beads (3-µm diameter) challenged with HUVECs were immunostained with rabbit anti-GST-antibody and Alexa-Fluor-568-labeled anti-rabbit-IgG antibody (red) before permeabilization, and were then permeabilized and immunostained with the anti-GST-antibody followed by Alexa-Fluor-488-labeled anti-rabbit-IgG antibody (green). Merge of red and green results in yellow color. A yellow cap on a bead (arrowhead) indicates partial internalization. Scale bar: 2 µm. (B′) Three-dimensional reconstruction of partially internalized bead. HUVECs transfected with the plasma membrane marker GFP–GPI (green) were challenged with 3-µm FnBPA beads for 30 min and immunostained for the extracellular portion of the beads using rabbit anti-GST-antibody and Alexa-Fluor-568-labeled secondary antibody (red). The antibody only stained the top part of the bead not enwrapped by plasma membrane giving rise to a cap-like structure. Scale bar: 2.5 µm (correlates with arrow lengths for all dimensions). (C) HUVECs treated without (control) or with siRNAs specific for luciferase (control siRNA) or Cdc42GAP (siRNAs no. 6 and 8) were transfected with vectors expressing either GFP–Cdc42GAP or GFP–Cdc42GAPΔGAP and then challenged with FnBPA beads (1-µm diameter) for 30 min. The percentage of partially internalized beads was determined as described in the Materials and Methods. Results represent mean±s.e.m.; at least 50–200 cells from three independent experiments were evaluated. **P<0.001, ***P<0.0001 (one-way ANOVA with Bonferroni's post test). (C′) Expression of GFP–Cdc42GAP constructs was verified by anti-GFP western blotting. (D) HUVECs treated with control siRNA or Cdc42GAP siRNA no. 8 (similar results were obtained with siRNA no. 6; K.H., data not shown) transfected with a vector for Myc–Cdc42 were subjected to GST–PAK-CRIB pulldown. Bound (active) Myc–Cdc42, the Myc–Cdc42 input and Cdc42GAP knockdown were assessed by western blotting. (E) HUVECs were transfected with empty vector (control) or with a vector for Myc–Cdc42-Q61L, or were treated with siRNAs specific for luciferase (control siRNA) or Cdc42 (no. 17) and then challenged with FnBPA beads (1-µm diameter) for 30 min. The percentage of partially internalized beads (left bar graph) and intracellular beads (right bar graph) was determined. Each bar represents mean±s.e.m. At least 150–200 cells from three independent experiments were evaluated. *P<0.05, **P<0.001, ***P<0.0001 (two-tailed, unpaired Student's t-test). A representative western blot shows the knockdown (KD) efficiency of Cdc42.

Cdc42GAP activity appears to be the transition of the phagocytic cup to the early phagosome, that is, the process of phagocytic cup closure.

We next asked whether the crucial role of Cdc42GAP in phagocytic cup closure is connected to its inhibitory effect on Cdc42. Pulldowns confirmed that Cdc42GAP knockdown artificially increases the level of active GTP-bound Cdc42 in HUVECs (Fig. 2D). To test whether Cdc42 that cannot be deactivated perturbs phagocytic cup closure, we overexpressed constitutively active Myc–Cdc42-Q61L in HUVECs before interaction with FnBPA beads. Myc–Cdc42-Q61L significantly increased the fraction of partially internalized FnBPA beads and consequently also reduced bead invasion (Fig. 2E). In contrast, overexpression of constitutively active Myc–Rac1-Q61L did not produce a phagocytic cup closure defect (Fig. S1D). In order to find out whether inhibition of Cdc42 also disturbs phagocytic cup closure we knocked it down by 52% by using siRNA. Cdc42 knockdown produced defects in phagocytic cup closure and bead invasion that were quantitatively similar to the effects of Cdc42GAP knockdown or Myc–Cdc42-Q61L overexpression (Fig. 2A,C,E).

These data indicate that a functioning activation–deactivation cycle of Cdc42 is required for efficient phagocytic cup closure during staphylococcal invasion and that Cdc42GAP adopts the deactivation part in this cycle.

Cdc42GAP terminates Cdc42-induced actin polymerization in phagocytic cups

We asked whether Cdc42GAP terminates actin polymerization stimulated by the invading bacteria. To visualize the spatiotemporal relation of Cdc42 recruitment and actin polymerization we co-expressed GFP–Cdc42 and the F-actin sensor Lifeact–mRFP in the cells and infected them with *FnBPA-S. carnosus*. Fluorescence intensity plots and images revealed that GFP–Cdc42 accumulation temporally and spatially mirrored Lifeact–mRFP accumulation at the bacteria (Fig. 3A). FRET experiments using a single-chain Cdc42 biosensor (Hanna et al., 2014) directly demonstrated Cdc42 activation in conjunction with actin polymerization at phagocytic cups (Fig. 3A′). The image series presented in Fig. 3A shows that actin polymerization proceeded in a typical biphasic manner as reported previously (Schroder et al., 2006). In comparison, when GFP–Cdc42GAP-R305A/6A was recruited by the staphylococci, actin polymerization in phagocytic cups started to decrease and the recruitment occurred in the form of vesicles (Fig. 3B). The sequential accumulation of Cdc42, F-actin and Cdc42GAP at phagocytic cups is consistent with the notion that Cdc42GAP turns off Cdc42-stimulated actin polymerization.

Attempts to directly visualize interplay of Cdc42 and Cdc42GAP at phagocytic cups in live cells failed due to strong adverse effects of co-expressing GFP–Cdc42 and mCherry–Cdc42GAP. Because the currently available anti-Cdc42 antibodies did not detect endogenous membrane-associated Cdc42, we expressed GFP–Cdc42, and in parallel immunostained endogenous Cdc42GAP in infected endothelial cells. As the data presented in Fig. 3A,B already infer, GFP–Cdc42 and Cdc42GAP were rarely found to colocalize at phagocytic cups and rather appeared to mutually exclude each other at this location (Fig. 3C). Furthermore, GFP–Cdc42 and Cdc42GAP both localized to the perinuclear region but did not colocalize there, likely reflecting the Golgi-associated pool of Cdc42 and the perinuclear recycling endosome pool of Cdc42GAP (Fig. S2A) (Erickson et al., 1996; Sirokmany et al., 2006). GFP–Cdc42 and Cdc42GAP also did not colocalize in the peripheral recycling endocytic vesicles (Fig. S2A). These data are consistent with a transient interaction of Cdc42GAP and Cdc42 at the plasma membrane sites triggered by integrin-activating bacteria forming phagocytic cups. The transient nature of this interaction can be explained well biochemically because Cdc42GAP rapidly dissociates from Cdc42 after GTP hydrolysis (Zhang et al., 1997).

To more directly test whether Cdc42GAP controls actin depolymerization in phagocytic cups, we imaged Lifeact–mRFP in Cdc42GAP-knockdown cells challenged with FnBPA beads (n=10 for each condition). Notably, upon Cdc42GAP knockdown, the duration of F-actin accumulation in phagocytic cups increased twofold (Fig. 3D,E,G). Furthermore, F-actin within the protracted phagocytic cups appeared to be more patchy and irregularly shaped when compared to controls (Fig. 3D,E). Protracted actin polymerization and irregularly shaped F-actin cups were also observed in cells expressing GFP–Cdc42-Q61L, suggesting that the effect of Cdc42GAP knockdown was caused by defective Cdc42 downregulation (Fig. 3F,G).

In summary, these data indicate that Cdc42GAP terminates Cdc42-induced actin polymerization in phagocytic cups formed by FnBPA-expressing staphylococci.

Journal of Cell Science (2016) 129, 2937-2949 doi:10.1242/jcs.186213

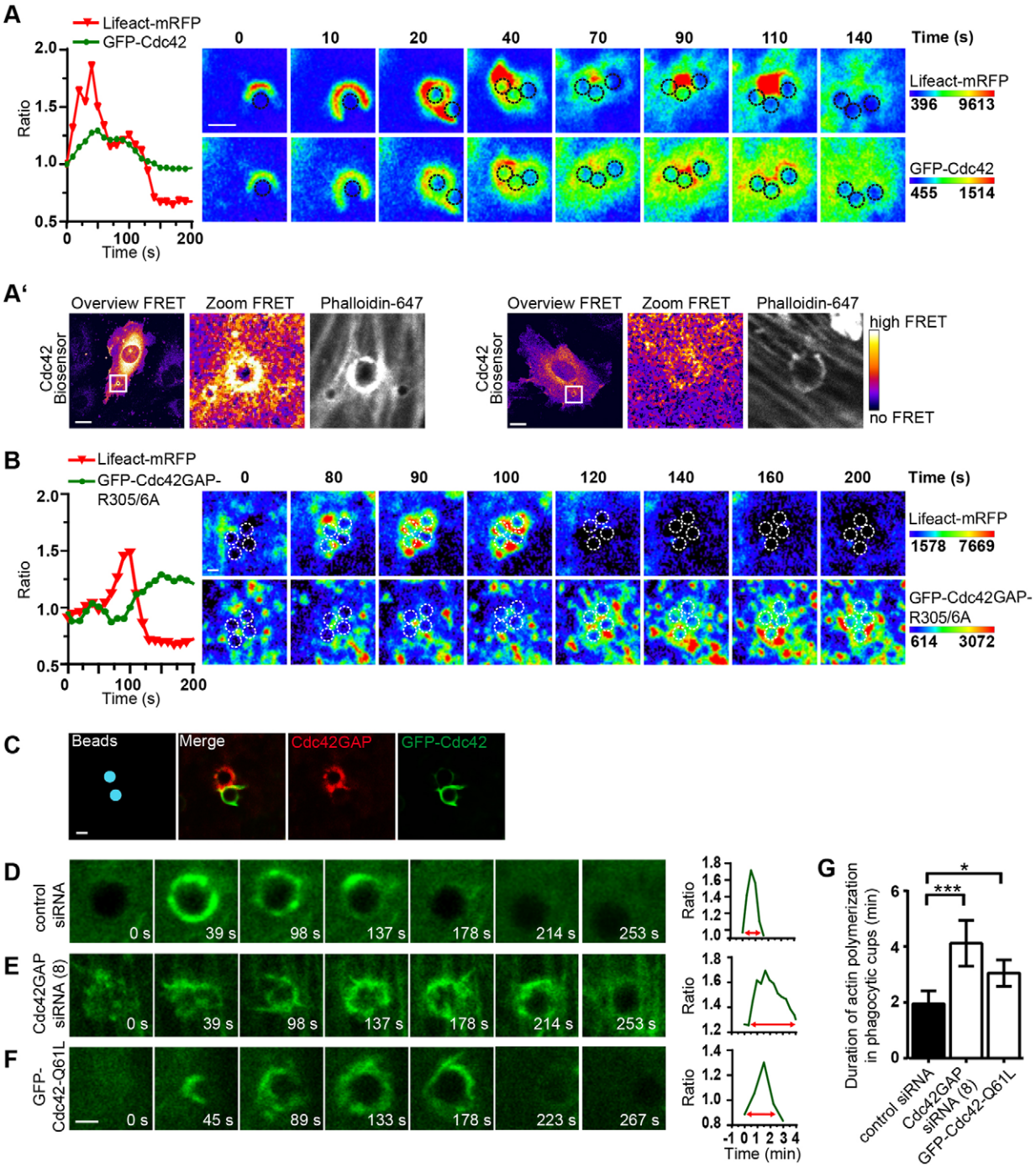

Fig. 3. Knockdown of Cdc42GAP and Cdc42 hyperactivation increase actin polymerization in FnBPA-triggered phagocytic cups. (A) HUVECs co-expressing Lifeact–mRFP and GFP–Cdc42 were infected with *FnBPA-S. camosus* and recorded by spinning disc live-cell microscopy. Fluorescence intensity kinetics of Lifeact–mRFP and GFP–Cdc42 at a bacterial cluster were assessed by employing the resulting time-lapse video (graph). In a series of confocal images from the video (Movie 1), single bacterial cells of the cluster are marked by dotted circles. GFP–Cdc42 and Lifeact–mRFP intensities are rainbow colored. Scale bar: 2 µm. (A′) HUVECs expressing the Cdc42 biosensor were challenged with a combination of 3-µm and 1-µm FnBPA beads and stained for actin with Phalloidin–Alexa-Fluor-647. Representative ratiometric images (FRET) were generated using the ImageJ Plug-in. FRET values are fire-colored, whereby blue and white correspond to no FRET and high FRET, respectively. The boxed region in overviews are depicted at a sevenfold enlargement in the zoom images. In the left panel, a high actin signal in a 3-µm bead phagocytic cup is associated with high FRET. In the right panel, a low actin signal is associated with low FRET. Scale bars: 10 µm. (B) Experiment was performed as in A but employing GFP–Cdc42GAP-R305/6A instead of GFP–Cdc42. Single bacterial cells of a cluster are marked by dotted circles. GFP–Cdc42GAP-R305/A and Lifeact–mRFP intensities are rainbow colored. Scale bar: 2 µm. (C) HUVECs expressing GFP–Cdc42 were challenged with FnBPA beads (3-µm diameter) for 30 min followed by immunostaining for Cdc42GAP (red). For better orientation, beads were pseudocolored in blue. Scale bar: 3 µm. (D–G) HUVECs were co-transfected with a vector expressing GFP–Lifeact or Lifeact–mRFP and (D) control siRNA, (E) Cdc42GAP siRNA (no. 8) or (F) a vector expressing GFP–Cdc42-Q61L and challenged with FnBPA beads (3-µm diameter). Cells were recorded by spinning disc live-cell microscopy and Lifeact intensity kinetics at the beads were assessed using the resulting time-lapse video (graphs). A series of confocal images from the videos are shown on the left. Scale bar: 2 µm. (G) Duration of actin polymerization in phagocytic cups was quantified. Each bar represents mean±s.d. of n=10 beads showing prominent Lifeact recruitment. *P<0.05, ***P<0.0001 (one-way ANOVA with Bonferroni's post test).

Journal of Cell Science (2016) 129, 2937-2949 doi:10.1242/jcs.186213

Cdc42GAP is delivered to phagocytic cups via recycling endocytic vesicles and the exocyst complex

We sought to identify the origin and spatiotemporal dynamics of the vesicles transporting Cdc42GAP to the phagocytic cup. To this end HUVECs expressing GFP–Cdc42GAP were infected with *FnBPA-S. carnosus* and investigated by live-cell imaging. Even though (over)expression of GFP–Cdc42GAP eventually decreased bacterial internalization, this construct better reflected intracellular Cdc42 dynamics than the arginine mutant construct. A representative recording clearly shows that recruitment of GFP–Cdc42GAP by a staphylococcal cluster occurs in the form of vesicles that dynamically move along the circumference of the cluster. The recording also suggests that the GFP–Cdc42GAP-positive vesicles originate in a perinuclear region (Fig. 4A; see Movie 1). Another recording demonstrates how Cdc42GAP-positive vesicles are reoriented towards an FnBPA bead shortly after it attaches to the cell surface (Fig. 4B; see Movie 2).

Cdc42GAP has been localized to transferrin-receptor- and Rab11-positive recycling endosomes in HeLa cells (Sirokmany et al., 2006). In HUVECs, endogenous Cdc42GAP and GFP–Rab11 colocalize in the perinuclear region, most certainly reflecting the endocytic recycling compartment (ERC), and in peripheral vesicles, representing recycling endocytic vesicles (Fig. 4C). Cdc42GAP-positive vesicles also colocalize with the recycling endocytic marker GFP–VAMP3 (Fig. S2B). It has been reported that tethering of recycling endocytic vesicles to the plasma membrane is regulated by the hetero-octameric exocyst complex (Rivera-Molina and Toomre, 2013; Takahashi et al., 2012). Accordingly, the exocyst component Sec15 colocalizes with Cdc42GAP and GFP–Rab11 in the ERC as well as in the recycling endocytic vesicles of HUVECs (Fig. 4C). Cdc42GAP did not colocalize with Rab5 (Fig. S2C). Exo70, Cdc42GAP and GFP–Rab11 also colocalized at phagocytic cups triggered by FNBPA beads (Fig. 4D). Sec8 and Sec15, other members of the exocyst complex, also colocalized with Cdc42GAP at phagocytic cups (see below Fig. 5B and L.R., unpublished observations). These data suggest that Cdc42GAP is delivered to phagocytic cups through recycling endocytic vesicles containing the exocyst complex.

We next asked whether the delivery of Cdc42GAP to phagocytic cups requires Rab11 and the exocyst complex. When Sec8 or Rab11 were knocked down in HUVECs, the recruitment of Cdc42GAP to FnBPA beads was significantly diminished (Fig. 5A–C; for intensity plots of the fluorescence signals at beads see Fig. S3A; for knockdown efficiencies see Fig. S4C,D). We reasoned that inhibition of Cdc42GAP delivery to the plasma membrane, the localization in the cell where it apparently interacts with Cdc42, should increase the level of active Cdc42. GST–PAK-CRIB pulldown experiments confirmed that both Exo70 and Rab11 knockdown caused a significant increase in the level of active Cdc42 (Fig. 5D,E; Fig. S3B). We further concluded that inhibition of Cdc42GAP delivery to the phagocytic cups should have a similar defect as Cdc42GAP knockdown, that is provoke a phagocytic cup closure defect. In fact, knockdown of Exo70 or Sec8 increased the percentage of FnBPA beads that were partially internalized to a similar degree to upon Cdc42GAP knockdown (Figs 5F and 2C). Consequently, bead internalization was also decreased after Exo70 or Sec8 knockdown (Fig. S3C). Binding of beads to cells was not affected by Sec8 knockdown (Fig. S1B). Consistent with this, Exo70 knockdown also increased the duration of actin polymerization in phagocytic cups by about twofold (Fig. S4A,B; for knockdown efficiency, see Fig. S4E). The effect of Sec8 knockdown was rescued by overexpression of Sec8–RFP but was not enhanced by concomitant knockdown of Cdc42GAP or Exo70 (Fig. 5G). Non-additive effects in the concomitant knockdowns Sec8 and Cdc42GAP, or Sec8 and Exo70 support the idea that the respective proteins act in the same regulatory pathway. Rab11 knockdown or expression of dominant-negative GFP–Rab11-S25N also produced a defect of phagocytic cup closure, yet to a smaller degree than Exo70- or Sec8 knockdown (Fig. 5H). Finally, overexpression of constitutively active GFP–Rab11-Q70L reversed the inhibitory effect of Exo70 knockdown on phagocytic cup closure (Fig. 5I). The effects on phagocytic cup closure described in Fig. 5G,H,I were concordant with effects on bacterial invasion (Fig. S3D,E,F). Taken together, these results provide further evidence that Rab11 and Exo70 act together in Cdc42GAP recruitment and phagocytic cup closure.

In summary, these results suggest that, during cell invasion, FnBPA-expressing staphylococci recruit Cdc42GAP by redirecting recycling endocytic vesicles to the phagocytic cup. The Cdc42GAP delivery involves the exocyst complex and downregulates Cdc42-induced actin polymerization in a spatially and temporally coordinated manner. This mechanism crucially determines timely and efficient phagocytic cup closure.

DISCUSSION

Integrin-mediated invasion of endothelial cells by *S. aureus* starts with the assembly of a focal-adhesion-like signaling complex at the bacteria–cell contact site (Geiger et al., 2009; Hauck et al., 2012; Schroder et al., 2006). This signaling complex induces actin polymerization through Rho GTP-binding proteins, N-WASp and the Arp2/3 complex. As a consequence, F-actin-rich phagocytic cups are formed that drive bacterial internalization (Freeman and Grinstein, 2014). Here, we describe that actin polymerization in the phagocytic cups is terminated by targeted delivery of the Cdc42 deactivator Cdc42GAP. This result demonstrates that, for bacterial invasion of cells, a process that closely resembles phagocytosis, not only activation but also deactivation of Cdc42 is essential. Recently, three different GAPs for the Rho GTP-binding proteins Rac and Rho were found to be involved in the Fcγ-receptor-dependent phagocytosis of large particles (>3–10 µm) by mouse macrophages (Schlam et al., 2015). Of note, we found that both artificial activation and deactivation of Cdc42 in the endothelial cells inhibited phagocytic cup closure and invasion. Thus, staphylococcal invasion requires the complete cycle of Cdc42 activation and deactivation. Rac behaves differently in this regard, because expression of constitutively active Rac1-Q61L did not alter FnBPA-mediated bacterial uptake. However, GAPs for Rac play a role in phagocytosis of larger objects (>3 µm diameter) by macrophages (Schlam et al., 2015). We noticed that knockdown of Cdc42GAP tended to produce a larger inhibitory effect on phagocytic cup closure than constitutively active Cdc42. This might suggest that other Cdc42 family GTP-binding proteins also regulated by Cdc42GAP, such as TC10 or TCL proteins, are additionally involved in bacterial invasion.

The Sec14-like domain of Cdc42GAP, which we found to be necessary and sufficient for phagocytic cup localization, binds to phosphatidylinositol-3-phosphate (Krugmann et al., 2002). This might potentially contribute to the reported effect of phosphoinositide 3-kinase, the enzyme that forms phosphatidylinositol-3-phosphate, on Cdc42 activity during phagocytosis (Beemiller et al., 2010).

We describe here that recycling endocytic vesicles deliver Cdc42GAP to phagocytic cups and that this is dependent on the

Journal of Cell Science (2016) 129, 2937-2949 doi:10.1242/jcs.186213

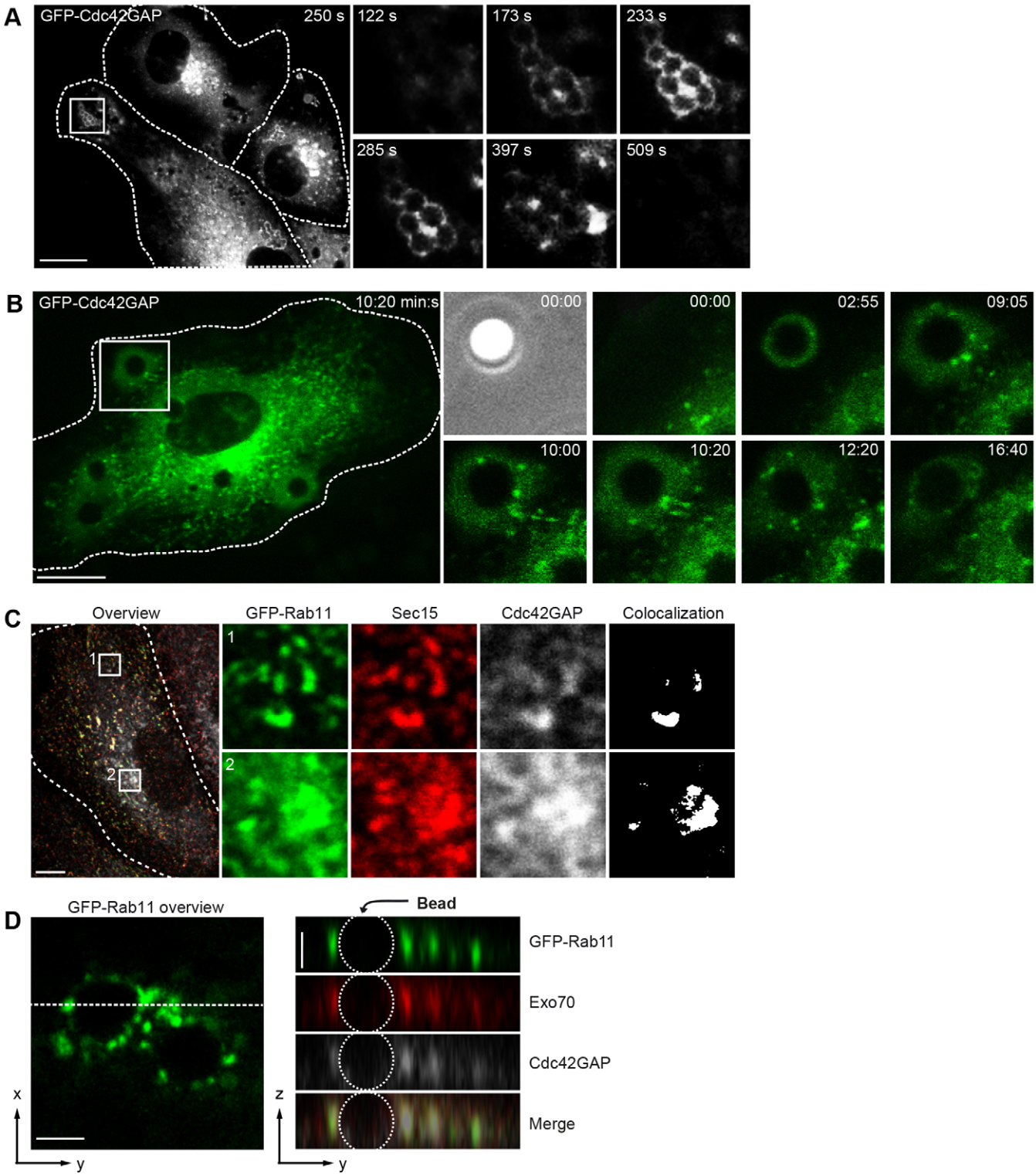

Fig. 4. Cdc42GAP resides in exocyst-positive recycling endocytic vesicles that are recruited to phagocytic cups. (A) HUVECs expressing GFP–Cdc42GAP were challenged with *FNBPA-S. carnosus* and recorded by spinning disc live-cell microscopy. Images were taken from a time-lapse movie (see Movie 1) at the indicated time points. The boxed area in the overview is depicted as a fourfold enlargement and over time in the right panel. Cell borders are indicated by broken lines. Scale bar: 10 µm. (B) HUVECs expressing GFP–Cdc42GAP were challenged with FnBPA beads (3-µm diameter) and recorded by spinning disc live-cell microscopy. Images were taken from a time-lapse movie (see Movie 2) at the indicated time points. The boxed area in the overview is depicted as a fourfold enlargement and over time in the right panel. Cell borders are indicated by broken lines. Scale bar: 10 µm. (C) HUVECs expressing GFP–Rab11 (green) were co-immunostained for Sec15 (red) and Cdc42GAP (gray). The boxed areas 1 in the periphery and 2 in the perinuclear region of the overview are depicted as a sixfold enlargement in the green, red and gray channels. Cell borders are outlined. White color represents structures in which all three proteins colocalize according to ImageJ analysis. Scale bar: 10 µm. (D) HUVECs expressing GFP–Rab11 (green) were challenged with FnBPA beads (3-µm diameter) for 30 min and co-immunostained for Exo70 (red) and Cdc42GAP (gray). GFP–Rab11, Exo70 and Cdc42GAP fluorescences and their merge (right panel) at an invading bead are shown in *z-y* projection along the dotted line from the GFP–Rab11 overview (left picture). Scale bar: 2.5 µm.

Journal of Cell Science (2016) 129, 2937-2949 doi:10.1242/jcs.186213

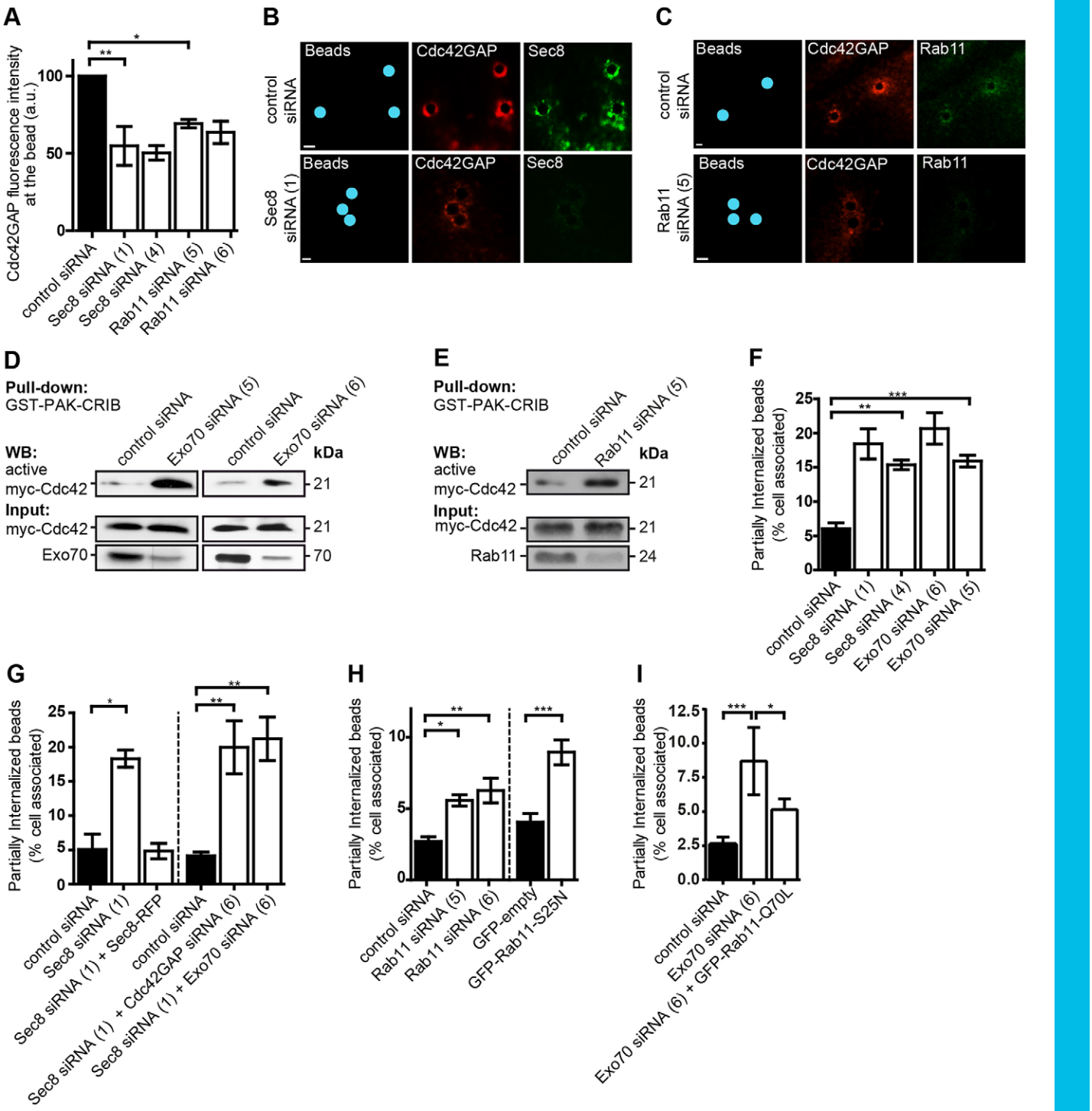

Fig. 5. Recruitment of Cdc42GAP through recycling endocytic vesicles and the exocyst regulates Cdc42 activity and phagocytic cup closure. (A) HUVECs were treated with control siRNA or siRNA specific for Sec8 (nos 1 or 4) or Rab11 (nos 5 or 6), challenged with FnBPA beads (3-µm diameter) for 30 min and immunostained for Cdc42GAP and either Sec8 or Rab11 (for knockdown efficiencies see Fig. S4C,D). Fluorescence intensity of immunostained Cdc42GAP at the beads was measured within a 6-µm diameter circle virtually placed around the beads using Volocity software. Each bar represents mean±s.d. for 150 beads from three independent experiments. *P<0.05, **P<0.001 (one-way ANOVA with Bonferroni's post test). (B,C) Representative immunofluorescence images of the experiments described in A. Beads were pseudocolored in blue. Scale bars: 2 µm. (D,E) HUVECs treated with control siRNA, Exo70 siRNA (nos 5 or 6) or Rab11 siRNA (no. 5) were transfected with a vector for Myc–Cdc42 and subjected to GST–PAK-CRIB pulldown. Bound (active) Myc-Cdc42, Myc–Cdc42 input and the Exo70- and Rab11 knockdown were assessed by western blotting (WB). (F–I) HUVECs were transfected with control siRNA, Sec8 siRNA (nos 1 or 4), Exo70 siRNA (nos 5 or 6), Cdc42GAP siRNA (no. 6), Rab11 siRNA (nos 5 or 6) in the indicated combinations or with a vector expressing GFP–Rab11-S25N or GFP. In rescue experiments, Sec8 siRNA (no. 1) and a vector expressing Sec8–RFP or Exo70 siRNA (no. 6), and a vector expressing GFP–Rab11-Q70L were co-transfected. Cells were challenged with FnBPA beads (1-µm diameter) for 30 min and the percentage of partially internalized beads was quantified as described in the Materials and Methods. Each bar represents mean±s.d. for 50–200 cells from three or four independent experiments. *P<0.005, **P<0.001, ***P<0.0001 (one-way ANOVA with Bonferroni's post test). For knockdown efficiencies see Fig. S4C–E.

Journal of Cell Science (2016) 129, 2937-2949 doi:10.1242/jcs.186213

exocyst complex. Although our data indicate that Cdc42 is downregulated by the exocyst-mediated delivery of Cdc42GAP, previous data has shown that Cdc42 reciprocally regulates the exocyst complex during bacterial invasion (Mohammadi and Isberg, 2013; Wu et al., 2008). Other work has shown that the exocyst complex controls the activity of the Rho GTP-binding proteins Rac and Rho through a presumed direct interaction with the Rac GAP SH3BP1 or the Rho GEF H1 (also known as ARHGEF2) with consequences for cell migration (Parrini et al., 2011) or vesicle trafficking (Pathak et al., 2012), respectively. Although we demonstrate here that the functional interaction of Cdc42GAP with Cdc42 requires the exocyst complex, we could not co-immunoprecipitate Cdc42GAP with any exocyst complex protein, nor could we detect a direct interaction of purified Cdc42GAP with any exocyst complex protein, despite intensive efforts. Rather, we provide evidence that the exocyst governs the interaction of Cdc42GAP and Cdc42 by targeting Cdc42GAP-harboring vesicles to Cdc42 at the plasma membrane. Plasma-membrane-bound Cdc42 is thought to constitute the active fraction of the protein (Aepfelbacher et al., 1994). At present, we cannot exclude that, as well as through recycling endocytic vesicles, Cdc42GAP is also delivered to phagocytic cups by an alternative mechanism or from a different subcellular pool.

In summary, our data integrated with previously published data suggest a regulatory circuit whereby Cdc42 activated by integrins at specific sites at the plasma membrane (Etienne-Manneville and Hall, 2001) stimulates the polarized recruitment of recycling endocytic vesicles with the help of the exocyst complex. The vesicles deliver Cdc42GAP, which then deactivates Cdc42 and thereby terminates further delivery of the vesicles and Cdc42GAP. Preliminary results from our laboratory suggest that this regulatory circuit might also control endothelial cell functions known to be instrumental in angiogenesis-like migration of endothelial cells and the formation of anastomoses between nascent endothelial cell tubules (Engelse et al., 2008; Koh et al., 2008, 2009).

Further investigation of the spatiotemporal coordination of Cdc42 activity, exocyst function and targeted Cdc42GAP delivery will provide a more comprehensive understanding of the dynamics of cell polarization during infection and other physiological processes.

MATERIALS AND METHODS

Cell culture and transfection

Human umbilical vein endothelial cells (HUVECs) were isolated from human umbilical cords (kindly provided by Marien-Krankenhaus, Hamburg, Germany) and cultured as described previously (Schroder et al., 2006). Approval for the analysis of anonymized umbilical cord donations was obtained by the Ethical Committee of the Ärztekammer Hamburg (Germany). Cells were cultured in endothelial cell growth medium (ECGM, PromoCell, Heidelberg, Germany) containing 0.05 µg/ml amphotericin B and 50 µg/ml gentamicin in a humidified 5% CO_2 atmosphere at 37°C and passaged every 4–6 days.

Cell transfection and siRNA experiments

Neon® Transfection System (Invitrogen, Darmstadt, Germany) was used to transfect HUVECs with 1 µg of plasmid DNA or siRNA according to the manufacturer's protocols. Human Cdc42GAP siRNAs (no. 6 and 8), human Cdc42 siRNA (no. 17), human Exo70 siRNA (no. 6), human Sec8 siRNA (no. 4) and human Rab11a siRNAs (no. 5 and 6) were obtained from Qiagen (Hilden, Germany). Human Sec8 siRNA (no. 1, 5′-CCUUGAUACCUCUCACUAU-3′) and human Exo70 siRNA (no. 5, 5′-UCGCAGAGAAGAAUCUACCUGUGUU-3′) were custom made and synthesized by Eurofins MWG Operon (Ebersberg, Germany). Control siRNA (against firefly luciferase) was obtained from Thermo Fisher (Waltham, USA).

DNA constructs

The human GST–Cdc42GAP construct was kindly provided by Alan Hall (Memorial Sloan-Kettering Cancer Center, New York City, NY). The Cdc42GAP gene (accession number NM_004308) was subcloned into pEGFP-C1 (Clontech, St.-Germain-en-Laye, France) and further used for construction of GFP–Cdc42GAP-R305/6A, GFP–Cdc42GAPΔGAP (amino acids 1–260), GFP–Cdc42GAPΔPPro (missing amino acids 227–239), GFP–Cdc42GAPΔSec14 (amino acids 208–440) and GFP–Cdc42GAPΔPProΔGAP (amino acids 1–208). GFP–Cdc42 was a kind gift of Klaudia Giehl (Justus-Liebig-University Giessen, Germany) and the Cdc42 gene (accession number BC003682) was subcloned into pRK5myc (BD Biosciences, Heidelberg, Germany). Myc–Cdc42-Q61L and Myc–Rac1-Q61L were kindly provided by Pontus Aspenström (Karolinska Institute, Stockholm, Sweden) and Cdc42-Q61L was subcloned into pEGFP-C1. GFP–Rab11, GFP–Rab11-Q70L and GFP–Rab11-S25N were provided by Stephen Ferguson (Robarts Research Institute, Ontario, Canada). GFP–Exo70 was a kind gift of Wei Guo (University of Pennsylvania, Philadelphia, PA), Sec8–RFP and GFP–Vamp3 were provided by Derek Toomre (Yale School of Medicine, New Haven, CT), GST–PAK-CRIB by John Collard (Netherlands Cancer Institute, Amsterdam, Netherlands) and Lifeact–mRFP was a kind gift of Michael Sixt (Max Planck Institute for Biochemistry, Munich, Germany; Riedl et al., 2008). pLifeAct-TagGFP2 was purchased from Ibidi (Ibidi, Munich, Germany). GST–FnBPA-DuD4 was as described previously (Schroder et al., 2006; Wiedemann et al., 2001). GFP–GPI was provided by Sergio Grinstein (Hospital for Sick Children, Toronto, Canada) and mcherry-N1 was purchased from Clontech. The Cdc42 single-chain biosensor harboring a mCerulean and mVenus FRET pair was a kind gift of Louis Hodgson (Albert Einstein College of Medicine, NY, USA) (Hanna et al., 2014). Control constructs harboring only the mCerulean donor or mVenus acceptor fluorophores were amplified by PCR and subcloned into pTriEX-HisMyc4 (Novagen, Merk Group, Darmstadt, Germany).

Antibodies

Production of monoclonal rat anti-Cdc42GAP antibody (RG39-A89) was performed using the human Cdc42GAP coding sequence (accession number NM_004308) and a previously described cDNA prime-protein boost strategy (Koch-Nolte et al., 2005). Rat anti-Cdc42GAP antibody (RG39-A89) was used at 1:200 and 1:5000 in immunofluorescence and western blotting, respectively. The rabbit anti-*Staphylococcus epidermidis* 5197 antiserum used to detect *S. carnosus* was generously provided by Holger Rohde (UKE Hamburg, Germany) and was used at 1:2000 in immunofluorescence. Staining of *S. aureus* was performed with commercially available rabbit anti-*S. aureus* antibody (1:2000, Biodesign International, Saco, ME). The monoclonal mouse anti-Exo70 antibody was a kind gift of Shu-Chan Hsu (Rutgers University, Piscataway, NJ; Vega and Hsu, 2001) and was used at 1:200 and 1:2000 for immunofluorescence and western blotting, respectively. Commercially available antibodies used in this study were: monoclonal rabbit anti-Rab5 (clone 1, cat. no. 3547, Cell Signaling, Frankfurt, Germany), used at 1:100 in immunofluorescence; monoclonal mouse anti-Sec8 (cat. no. 610658, BD Biosciences, Heidelberg, Germany), used at 1:200 in immunofluorescence and 1:4000 in western blotting; monoclonal rabbit anti-Cdc42 (clone 11A11, cat. no. 2466, Cell Signaling), used at 1:1000 in western blotting; monoclonal mouse anti-Rab11a (clone 47, cat. no. 610656, BD Transduction Laboratories, Heidelberg, Germany), used at 1:1000 in western blotting; abd monoclonal rabbit anti-Rab11 D4F5 (cat. no. 5589, Cell Signaling), used at 1:100 in immunofluorescence. GST was detected using rabbit pAb A5800 from Invitrogen at 1:250 in immunofluorescence, and monoclonal mouse anti-myc (clone 9B11, cat. no. 2276, Cell Signaling) was used 1:200 and 1:3000 in immunofluorescence and western blotting, respectively. Mouse monoclonal anti-β-actin MAB1501 (clone C4) was purchased from Millipore (Schwalbach, Germany) and used 1:5000 in western blotting. Monoclonal mouse anti-GFP antibody (clone JL-8, cat. no. 632381, Takara Bio/Clontech, St-Germain-en-Laye, France) was used 1:5000 in western blotting. Phalloidin coupled to Alexa Fluor 647 (Invitrogen) was used 1:500 in immunofluorescence. Secondary antibodies used for immunofluorescence staining were Alexa-Fluor-488-, Alexa-Fluor-568-

or Alexa-Fluor-647-labeled goat anti-mouse-IgG, goat anti-rabbit-IgG or goat anti-rat-IgG (Molecular Probes, Karlsruhe, Germany), used at 1:200. Secondary antibodies for western blotting were horseradish-peroxidase-linked goat anti-mouse-IgG, goat anti-rabbit-IgG and goat anti-rat-IgG (GE Healthcare, Munich, Germany), used at 1:50,000.

Immunofluorescence staining

HUVECs cultured on glass coverslips (12 mm diameter, Hartenstein, Germany) were fixed with 3.7% (v/v) formaldehyde in phosphate-buffered saline (PBS) for 10 min and permeabilized with 0.1% (v/v) Triton X-100 in PBS for 10 min. Unspecific binding sites were blocked by incubation with 1% (w/v) bovine serum albumin (BSA) in PBS for 30 min. Cells were incubated with primary antibody for 1 h, washed three times using PBS, followed by incubation with a 1:200 dilution of secondary antibody for 45 min. Antibody dilutions were prepared in 1% BSA solution. Washed coverslips were air dried and mounted in MOWIOL (Calbiochem, Darmstadt, Germany).

Bacterial strains and culture conditions

All staphylococcal strains were as described previously (Sinha et al., 2000). *S. aureus* strain Cowan I and *S. aureus* strain 8325-4 were cultured in tryptic soy broth (TSB). *S. aureus* strain DU5883 is an isogenic mutant of strain 8325-4 with deletions in FnBPA and FnBPB, and was cultured in TSB containing 20 µg/ml tetracycline and 5 µg/ml erythromycin. DU5883 complemented with the plasmids pFnBPA4 or pFnBPB4 was cultured in TSB containing 20 µg/ml tetracycline, 5 µg/ml erythromycin and 20 µg/ml chloramphenicol. Wild-type *S. carnosus* strain TM300 and that strain expressing FnBPA from *S. aureus* strain 8325-3 (*FnBPA-S. carnosus*) were cultured in TSB or TSB containing 20 µg/ml chloramphenicol, respectively.

Interaction of HUVECs with latex beads or bacteria

Production of GST or GST–FnBPA-DuD4 and coating of polystyrene latex beads (1- or 3-µm diameter, Polyscience Inc, Eppelheim, Germany) was as described previously (Schroder et al., 2006; Wiedemann et al., 2001). An adequate volume of coated-bead slurry was incubated with 2.5×10^5 HUVECs grown on glass coverslips in 12-well plates at 37°C for 30 min to obtain a multiplicity of infection (MOI) of 10. Overnight cultures of *S. aureus*- or *S. carnosus* strains were grown in TSB containing antibiotics at 37°C. Confluent HUVEC monolayers grown in antibiotic-free medium were infected with bacteria at a MOI of 10 at 37°C for 30 min.

Invasion assay

HUVECs were incubated with coated-beads or bacteria, fixed with 3.7% paraformaldehyde for 10 min and blocked with 1% BSA in PBS for 30 min. For quantitative analysis of extracellular, intracellular and partially internalized beads or bacteria, cells were incubated with primary rabbit antibodies against staphylococcal or *S. aureus* cells (1:2000 dilution, 1 h) or rabbit anti-GST antibodies (1:250 dilution, 1 h), and subsequently incubated with secondary anti-rabbit-IgG antibody coupled to Alexa Fluor 568 (1:200 dilution, 45 min) to stain only extracellular particles. Thereafter, cells were permeabilized with 0.1% Triton X-100, blocked with 1% BSA followed by a second round of staining with anti-staphylococcal- or anti-GST antibodies and secondary anti-rabbit-IgG antibody coupled to Alexa Fluor 488. When GFP fusion constructs were expressed in parallel, the second round of staining was performed with secondary anti-rabbit-IgG antibody coupled to Alexa Fluor 647 (1:200 dilution, 45 min). The number of extracellular, intracellular and partially internalized beads was counted manually by visual inspection of insular beads.

Microscopy and image analysis

Fixed samples and Cdc42 biosensor were analyzed with a confocal laser-scanning microscope (Leica DMI 6000 with a Leica TCS SP5 AOBS® confocal point scanner) equipped with a 63× oil-immersion HCX PL APO CS objective (NA 1.4-0.6). Leica LAS AF software (Leica Microsystems, Wetzlar, Germany) was used for acquisition. For FRET experiments mCerulean (excitation 458 nm, emission 475-495 nm), mVenus (excitation 514 nm, emission 535-555 nm) and FRET fluorescence intensities (excitation 458 nm, emission 535–555 nm) were sequentially recorded using appropriate filter sets. Bleedthrough calibration was performed by expressing only the individual mCerulean or the mVenus constructs (see above). FRET calculation was performed using FRET and colocalization analyzer plug-in (Hachet-Haas et al., 2006) run on ImageJ (NIH, Bethesda, MD). The FRET image in 'fire'-color displays intensities of acceptor emission due to FRET in each pixel. For confocal time-lapse microscopy, HUVECs were transfected and seeded onto glass-bottom dishes (MatTek, Ashland, USA) at least 1 day before the experiment. Images were acquired with a Zeiss Axiovert 200 M stand equipped with a spinning disk confocal unit (Yokogawa CSU22, Tokyo, Japan), a 63× Plan-Apochromat Ph3 oil NA 1.4 objective (Carl Zeiss, Jena, Germany), an EM-CCD camera (Hamamatsu C9100-02, Hamamatsu City, Japan), and a temperature- and CO_2-controllable environmental chamber (Solent Scientific, Regensworth, UK). Acquisition and processing of images was performed with Volocity Software (Improvision, Coventry, UK). Mean fluorescence intensity was quantified within circular regions of interest (6-µm diameter) virtually placed around beads and bead-free areas, respectively, using Volocity software. Intensity plots were generated by measuring the fluorescence intensity along the indicated arrows. A ratio of the obtained fluorescence intensity values versus a fluorescence intensity from an equal arrow in a bead- or bacteria-free region was determined using Volocity software. The colocalization plug-in of ImageJ software was used to visualize structures in which GFP–Rab11, Cdc42GAP and Sec15 colocalized, excluding structures containing only one or two proteins.

Cdc42 activity pulldown

The GST-tagged Cdc42- and Rac-interactive binding (CRIB) domain of PAK (GST-PAK-CRIB) was purified from *E. coli* BL21 and incubated with HUVECs lysed in 150 mM NaCl, 50 mM Tris-HCl pH 7.4, 5 mM $MgCl_2$, 1% Triton X-100 and protease inhibitors, at 4°C for 2.5 h as described previously (Ogita and Takai, 2006). The amount of Myc–Cdc42 pulled down by GST–PAK-CRIB (active Myc–Cdc42) was determined by western blotting.

Western blotting

Proteins separated by SDS-PAGE were transferred to polyvinylidene difluoride membrane (Immobilion-P, Millipore, Schwalbach, Germany) by semi-dry blotting. The membrane was incubated in blocking solution (5% milk powder in Tris-buffered saline, 0.1% Tween 20) for at least 30 min, followed by incubation with primary and horseradish-peroxidase-conjugated secondary antibodies, chemiluminescence detection (SuperSignal Pico or SuperSignal West Femto, Pierce Chemicals) and signal visualization on X-ray films (Fujifilm, Düsseldorf, Germany).

Statistical analysis

Statistical analysis was performed using GraphPad Prism 5 and 6 (GraphPad Software, La Jolla, USA) using one-way ANOVA with Bonferroni's post test or two-tailed, unpaired Student's *t*-tests; both with 95% confidence interval.

Acknowledgements

We thank Virgilio Antonio Failla and Bernd Zobiak from the UKE Microscopy Imaging Facility (UMIF) for help with microscopic experiments and Gudrun Dubberke and Fabienne Seyfried for help with antibody generation.

Competing interests

The authors declare no competing or financial interests.

Author contributions

L.R., K.H., C.T., A.R. and B.S. designed and performed experiments. F.K.-N., F.R.-M. and D.T. contributed essential materials. D.T. and F.R.-M. evaluated data and aided in writing the manuscript. M.A. conceived experiments, evaluated data and wrote the manuscript. This work is part of the doctoral thesis of K.H.

Funding

Work was supported by PhD scholarships from the Leibniz Graduate School (Model systems for infectious diseases to K.H.); and from Deutsche Forschungsgemeinschaft [grant number GRK-1459 to A.R. and L.R.]. This work

was also supported by the National Institutes of Health [grant number R01GM098498-01 to D.T.]. Deposited in PMC for release after 12 months.

Supplementary information

Supplementary information available online at
http://jcs.biologists.org/lookup/doi/10.1242/jcs.186213.supplemental

References

Aepfelbacher, M., Vauti, F., Weber, P. C. and Glomset, J. A. (1994). Spreading of differentiating human monocytes is associated with a major increase in membrane-bound CDC42. *Proc. Natl. Acad. Sci. USA* **91**, 4263-4267.

Barfod, E. T., Zheng, Y., Kuang, W. J., Hart, M. J., Evans, T., Cerione, R. A. and Ashkenazi, A. (1993). Cloning and expression of a human CDC42 GTPase-activating protein reveals a functional SH3-binding domain. *J. Biol. Chem.* **268**, 26059-26062.

Beemiller, P., Zhang, Y., Mohan, S., Levinsohn, E., Gaeta, I., Hoppe, A. D. and Swanson, J. A. (2010). A Cdc42 activation cycle coordinated by PI 3-kinase during Fc receptor-mediated phagocytosis. *Mol. Biol. Cell* **21**, 470-480.

Carabeo, R. (2011). Bacterial subversion of host actin dynamics at the plasma membrane. *Cell. Microbiol.* **13**, 1460-1469.

Chorianopoulos, E., Bea, F., Katus, H. A. and Frey, N. (2009). The role of endothelial cell biology in endocarditis. *Cell Tissue Res.* **335**, 153-163.

Deanfield, J. E., Halcox, J. P. and Rabelink, T. J. (2007). Endothelial function and dysfunction: testing and clinical relevance. *Circulation* **115**, 1285-1295.

Edwards, A. M. and Massey, R. C. (2011). How does Staphylococcus aureus escape the bloodstream? *Trends Microbiol.* **19**, 184-190.

Engelse, M. A., Laurens, N., Verloop, R. E., Koolwijk, P. and van Hinsbergh, V. W. M. (2008). Differential gene expression analysis of tubule forming and non-tubule forming endothelial cells: CDC42GAP as a counter-regulator in tubule formation. *Angiogenesis* **11**, 153-167.

Erickson, J. W., Zhang, C., Kahn, R. A., Evans, T. and Cerione, R. A. (1996). Mammalian Cdc42 is a brefeldin A-sensitive component of the Golgi apparatus. *J. Biol. Chem.* **271**, 26850-26854.

Etienne-Manneville, S. (2004). Cdc42–the centre of polarity. *J. Cell Sci.* **117**, 1291-1300.

Etienne-Manneville, S. and Hall, A. (2001). Integrin-mediated activation of Cdc42 controls cell polarity in migrating astrocytes through PKCζ. *Cell* **106**, 489-498.

Freeman, S. A. and Grinstein, S. (2014). Phagocytosis: receptors, signal integration, and the cytoskeleton. *Immunol. Rev.* **262**, 193-215.

Geiger, B., Spatz, J. P. and Bershadsky, A. D. (2009). Environmental sensing through focal adhesions. *Nat. Rev. Mol. Cell Biol.* **10**, 21-33.

Goldenberg, N. M., Steinberg, B. E., Slutsky, A. S. and Lee, W. L. (2011). Broken barriers: a new take on sepsis pathogenesis. *Sci. Transl. Med.* **3**, 88ps25.

Hachet-Haas, M., Converset, N., Marchal, O., Matthes, H., Gioria, S., Galzi, J.-L. and Lecat, S. (2006). FRET and colocalization analyzer—A method to validate measurements of sensitized emission FRET acquired by confocal microscopy and available as an ImageJ Plug-in. *Microsc. Res. Tech.* **69**, 941-956.

Hanna, S., Miskolci, V., Cox, D. and Hodgson, L. (2014). A new genetically encoded single-chain biosensor for Cdc42 based on FRET, useful for live-cell imaging. *PLoS ONE* **9**, e96469.

Hauck, C. R., Borisova, M. and Muenzner, P. (2012). Exploitation of integrin function by pathogenic microbes. *Curr. Opin. Cell Biol.* **24**, 637-644.

Hertzog, M. and Chavrier, P. (2011). Cell polarity during motile processes: keeping on track with the exocyst complex. *Biochem. J.* **433**, 403-409.

Kerrigan, S. W. and McDonnell, C. (2015). Dysregulation of the endothelium following Staphylococcus aureus infection. *Biochem. Soc. Trans.* **43**, 715-719.

Kim, K. S. (2008). Mechanisms of microbial traversal of the blood-brain barrier. *Nat. Rev. Microbiol.* **6**, 625-634.

Koch-Nolte, F., Glowacki, G., Bannas, P., Braasch, F., Dubberke, G., Ortolan, E., Funaro, A., Malavasi, F. and Haag, F. (2005). Use of genetic immunization to raise antibodies recognizing toxin-related cell surface ADP-ribosyltransferases in native conformation. *Cell. Immunol.* **236**, 66-71.

Koh, W., Mahan, R. D. and Davis, G. E. (2008). Cdc42- and Rac1-mediated endothelial lumen formation requires Pak2, Pak4 and Par3, and PKC-dependent signaling. *J. Cell Sci.* **121**, 989-1001.

Koh, W., Sachidanandam, K., Stratman, A. N., Sacharidou, A., Mayo, A. M., Murphy, E. A., Cheresh, D. A. and Davis, G. E. (2009). Formation of endothelial lumens requires a coordinated PKCepsilon-, Src-, Pak- and Raf-kinase-dependent signaling cascade downstream of Cdc42 activation. *J. Cell Sci.* **122**, 1812-1822.

Krugmann, S., Anderson, K. E., Ridley, S. H., Risso, N., McGregor, A., Coadwell, J., Davidson, K., Eguinoa, A., Ellson, C. D., Lipp, P. et al. (2002). Identification of ARAP3, a novel PI3K effector regulating both Arf and Rho GTPases, by selective capture on phosphoinositide affinity matrices. *Mol. Cell* **9**, 95-108.

Lancaster, C. A., Taylor-Harris, P. M., Self, A. J., Brill, S., van Erp, H. E. and Hall, A. (1994). Characterization of rhoGAP. A GTPase-activating protein for rho-related small GTPases. *J. Biol. Chem.* **269**, 1137-1142.

Laschke, M. W., Kerdudou, S., Herrmann, M. and Menger, M. D. (2005). Intravital fluorescence microscopy: a novel tool for the study of the interaction of Staphylococcus aureus with the microvascular endothelium in vivo. *J. Infect. Dis.* **191**, 435-443.

Lee, W. L. and Slutsky, A. S. (2010). Sepsis and endothelial permeability. *N. Engl. J. Med.* **363**, 689-691.

Lemichez, E., Lecuit, M., Nassif, X. and Bourdoulous, S. (2010). Breaking the wall: targeting of the endothelium by pathogenic bacteria. *Nat. Rev. Microbiol.* **8**, 93-104.

Lerm, M., Brodin, V. P., Ruishalme, I., Stendahl, O. and Särndahl, E. (2007). Inactivation of Cdc42 is necessary for depolymerization of phagosomal F-actin and subsequent phagosomal maturation. *J Immunol.* **178**, 7357-7365.

Letinic, K., Sebastian, R., Toomre, D. and Rakic, P. (2009). Exocyst is involved in polarized cell migration and cerebral cortical development. *Proc. Natl. Acad. Sci. USA* **106**, 11342-11347.

Lowy, F. D. (1998). Staphylococcus aureus infections. *N. Engl. J. Med.* **339**, 520-532.

Mohammadi, S. and Isberg, R. R. (2013). Cdc42 interacts with the exocyst complex to promote phagocytosis. *J. Cell Biol.* **200**, 81-93.

Munson, M. and Novick, P. (2006). The exocyst defrocked, a framework of rods revealed. *Nat. Struct. Mol. Biol.* **13**, 577-581.

Ogita, H. and Takai, Y. (2006). Activation of Rap1, Cdc42, and rac by nectin adhesion system. *Methods Enzymol.* **406**, 415-424.

Orchard, R. C., Kittisopikul, M., Altschuler, S. J., Wu, L. F., Süel, G. M. and Alto, N. M. (2012). Identification of F-actin as the dynamic hub in a microbial-induced GTPase polarity circuit. *Cell* **148**, 803-815.

Parrini, M. C., Sadou-Dubourgnoux, A., Aoki, K., Kunida, K., Biondini, M., Hatzoglou, A., Poullet, P., Formstecher, E., Yeaman, C., Matsuda, M. et al. (2011). SH3BP1, an exocyst-associated RhoGAP, inactivates Rac1 at the front to drive cell motility. *Mol. Cell* **42**, 650-661.

Pathak, R., Delorme-Walker, V. D., Howell, M. C., Anselmo, A. N., White, M. A., Bokoch, G. M. and Dermardirossian, C. (2012). The microtubule-associated Rho activating factor GEF-H1 interacts with exocyst complex to regulate vesicle traffic. *Dev. Cell* **23**, 397-411.

Que, Y.-A., Haefliger, J.-A., Piroth, L., François, P., Widmer, E., Entenza, J. M., Sinha, B., Herrmann, M., Francioli, P. and Vaudaux, P. (2005). Fibrinogen and fibronectin binding cooperate for valve infection and invasion in Staphylococcus aureus experimental endocarditis. *J. Exp. Med.* **201**, 1627-1635.

Rauch, L., Hennings, K. and Aepfelbacher, M. (2014). A role for exocyst in maturation and bactericidal function of staphylococci-containing endothelial cell phagosomes. *Traffic* **15**, 1083-1098.

Riedl, J., Crevenna, A. H., Kessenbrock, K., Yu, J. H., Neukirchen, D., Bista, M., Bradke, F., Jenne, D., Holak, T. A., Werb, Z. et al. (2008). Lifeact: a versatile marker to visualize F-actin. *Nat. Methods* **5**, 605-607.

Rivera-Molina, F. and Toomre, D. (2013). Live-cell imaging of exocyst links its spatiotemporal dynamics to various stages of vesicle fusion. *J. Cell. Biol.* **201**, 673-680.

Schlam, D., Bagshaw, R. D., Freeman, S. A., Collins, R. F., Pawson, T., Fairn, G. D. and Grinstein, S. (2015). Phosphoinositide 3-kinase enables phagocytosis of large particles by terminating actin assembly through Rac/Cdc42 GTPase-activating proteins. *Nat. Commun.* **6**, 8623.

Schroder, A., Schroder, B., Roppenser, B., Linder, S., Sinha, B., Fassler, R. and Aepfelbacher, M. (2006). Staphylococcus aureus fibronectin binding protein-A induces motile attachment sites and complex actin remodeling in living endothelial cells. *Mol. Biol. Cell* **17**, 5198-5210.

Shen, Y., Li, N., Wu, S., Zhou, Y., Shan, Y., Zhang, Q., Ding, C., Yuan, Q., Zhao, F., Zeng, R. et al. (2008). Nudel binds Cdc42GAP to modulate Cdc42 activity at the leading edge of migrating cells. *Dev. Cell* **14**, 342-353.

Sinha, B., Francois, P. P., Nusse, O., Foti, M., Hartford, O. M., Vaudaux, P., Foster, T. J., Lew, D. P., Herrmann, M. and Krause, K. H. (1999). Fibronectin-binding protein acts as Staphylococcus aureus invasin via fibronectin bridging to integrin alpha5beta1. *Cell. Microbiol.* **1**, 101-117.

Sinha, B., Francois, P., Que, Y.-A., Hussain, M., Heilmann, C., Moreillon, P., Lew, D., Krause, K.-H., Peters, G. and Herrmann, M. (2000). Heterologously expressed Staphylococcus aureus fibronectin-binding proteins are sufficient for invasion of host cells. *Infect. Immun.* **68**, 6871-6878.

Sirokmany, G., Szidonya, L., Káldi, K., Gáborik, Z., Ligeti, E. and Geiszt, M. (2006). Sec14 homology domain targets p50RhoGAP to endosomes and provides a link between Rab and Rho GTPases. *J. Biol. Chem.* **281**, 6096-6105.

Symons, M. and Settleman, J. (2000). Rho family GTPases: more than simple switches. *Trends Cell Biol.* **10**, 415-419.

Szczur, K., Xu, H., Atkinson, S., Zheng, Y. and Filippi, M.-D. (2006). Rho GTPase CDC42 regulates directionality and random movement via distinct MAPK pathways in neutrophils. *Blood* **108**, 4205-4213.

Takahashi, S., Kubo, K., Waguri, S., Yabashi, A., Shin, H.-W., Katoh, Y. and Nakayama, K. (2012). Rab11 regulates exocytosis of recycling vesicles at the plasma membrane. *J. Cell Sci.* **125**, 4049-4057.

Vega, I. E. and Hsu, S. C. (2001). The exocyst complex associates with microtubules to mediate vesicle targeting and neurite outgrowth. *J. Neurosci.* **21**, 3839-3848.

Vestweber, D. (2015). How leukocytes cross the vascular endothelium. *Nat. Rev. Immunol.* **15**, 692-704.

Wang, L., Yang, L., Burns, K., Kuan, C.-Y. and Zheng, Y. (2005). Cdc42GAP regulates c-Jun N-terminal kinase (JNK)-mediated apoptosis and cell number during mammalian perinatal growth. *Proc. Natl. Acad. Sci. USA* **102**, 13484-13489.

Wang, L., Yang, L., Filippi, M.-D., Williams, D. A. and Zheng, Y. (2006). Genetic deletion of Cdc42GAP reveals a role of Cdc42 in erythropoiesis and hematopoietic stem/progenitor cell survival, adhesion, and engraftment. *Blood* **107**, 98-105.

Wiedemann, A., Linder, S., Grassl, G., Albert, M., Autenrieth, I. and Aepfelbacher, M. (2001). Yersinia enterocolitica invasin triggers phagocytosis via beta1 integrins, CDC42Hs and WASp in macrophages. *Cell. Microbiol.* **3**, 693-702.

Wu, H., Rossi, G. and Brennwald, P. (2008). The ghost in the machine: small GTPases as spatial regulators of exocytosis. *Trends Cell Biol.* **18**, 397-404.

Yang, L., Wang, L. and Zheng, Y. (2006). Gene targeting of Cdc42 and Cdc42GAP affirms the critical involvement of Cdc42 in filopodia induction, directed migration, and proliferation in primary mouse embryonic fibroblasts. *Mol. Biol. Cell* **17**, 4675-4685.

Zhang, B., Wang, Z.-X. and Zheng, Y. (1997). Characterization of the interactions between the small GTPase Cdc42 and its GTPase-activating proteins and putative effectors. Comparison of kinetic properties of Cdc42 binding to the Cdc42-interactive domains. *J. Biol. Chem.* **272**, 21999-22007.